Nanoscale

PAPER

View Article Online
View Journal | View Issue

Cite this: *Nanoscale*, 2017, **9**, 7419

Advanced microscopy and spectroscopy reveal the adsorption and clustering of Cu(II) onto TEMPO-oxidized cellulose nanofibers†

Chuantao Zhu,[a,b] Alexander Soldatov[b] and Aji P. Mathew *[a,b]

TEMPO (2,2,6,6-tetramethylpiperidine-1-oxylradical)-mediated oxidation nanofibers (TOCNF), as a biocompatible and bioactive material, have opened up a new application of nanocellulose for the removal of water contaminants. This development demands extremely sensitive and accurate methods to understand the surface interactions between water pollutants and TOCNF. In this report, we investigated the adsorption of metal ions on TOCNF surfaces using experimental techniques atthe nano and molecular scales with Cu(II) as the target pollutant in both aqueous and dry forms. Imaging with *in situ* atomic force microscopy (AFM), together with a study of the physiochemical properties of TOCNF caused by adsorption with Cu(II) in liquid, were conducted using the PeakForce Quantitative NanoMechanics (PF-QNM) mode at the nano scale. The average adhesion force between the tip and the target single TOCNF almost tripled after adsorption with Cu(II) from 50 pN to 140 pN. The stiffness of the TOCNF was also enhanced because the Cu(II) bound to the carboxylate groups and hardened the fiber. AFM topography, scanning electron microscopy-energy dispersive X-ray spectroscopy (SEM-EDS) mapping and X-ray photoelectron spectroscopy (XPS) indicated that the TOCNF were covered by copper nanolayers and/or nanoparticles after adsorption. The changes in the molecular structure caused by the adsorption were demonstrated by Raman and attenuated total reflectance-Fourier transform infrared spectroscopy (ATR-FTIR). This methodology will be of great assistance to gain qualitative and quantitative information on the adsorption process and interaction between charged entities in aqueous medium.

Received 3rd March 2017,
Accepted 25th April 2017

DOI: 10.1039/c7nr01566f

rsc.li/nanoscale

Introduction

Nanocellulose and cellulosic substrates used as contaminant adsorbents have attracted increased attention for their environmental engineering applications in recent years.[1,2] Owing to the hierarchical structure and tailorable adsorption behavior *via* subsequent surface chemical modification[2,3] with carboxylic, sulfate and phosphate groups,[4] nanocellulose is not only a biocompatible but also a bioactive material[5] and shows excellent potential as a promising carrier material for the immobilization of water pollutants such as dyes,[6,7] pesticides,[8] bacteria and viruses,[9] and a wide range of heavy metal ions, including Ag(I),[10] U(II),[11] Fe(III), Cu(II),[12] Ni(II), Cr(III) and Zn(II).[13]

TEMPO (2,2,6,6-tetramethylpiperidine-1-oxylradical)-mediated oxidation nanofibers (TOCNF), a new bio-based nano-material prepared from abundantly available wood biomass by the position-selective catalytic oxidation of C6 primary hydroxyls,[14] have opened up a new application of nanocellulose for the removal of water contaminants. By using TOCNF as a reaction template, Ifuku's group found stable silver nanoparticles with a narrow size distribution and high density through ion interactions between the host carboxylate groups and the guest Ag(I) along the nanofibers.[15] The carboxyl and hydroxyl groups of carboxylated cellulose nanocrystals supplied a coordination effect to adsorb metallic cations and Ag nanoparticles.[16] In our recent research activities,[17,18] the use of TOCNF for the adsorption of heavy metal ions (Cu(II)) from contaminated water and the adsorption capacity and selectivity were extensively investigated and have shown promising results.[13,19] Cu(II) adsorption capacities at various initial Cu(II) concentrations from 2–250 mg L^{-1} were investigated.[19] Meanwhile, copper nanoparticles with a size of around 100 nm were found on the surface of the dry TOCNF samples after adsorption.

[a]*Department of Materials and Environmental Chemistry, Stockholm University, 10691 Stockholm, Sweden. E-mail: aji.mathew@mmk.su.se*
[b]*Department of Engineering Sciences and Mathematics, Luleå University of Technology, 97187 Luleå, Sweden*

†Electronic supplementary information (ESI) available: Zeta-potential of TOCNF and TOCNF + Cu in nitric acid solution at different pH values, Raman intensity variations of wood and TOCNF around wavenumber 1590–1595 cm^{-1} before and after adsorption, and schematic structure of the TOCNF unit with COO^- groups in both dry and liquid media. See DOI: 10.1039/c7nr01566f

Atomic force microscopy (AFM) is a powerful tool and has made possible the direct examination of the morphological and mechanical properties of substrates for the *in situ* study of adsorption processes.[20,21] AFM visualizes the topography of surfaces with the formation of adsorbed layers[22,23] or particles[24] from the model environment. Adhesion and repulsion forces caused by surface interactions between colloidal probes and substrates are precisely detected and used for interpreting adsorption behavior.[10,25] The mechanical properties of the substrates like the Young's modulus,[26,27] deformation, dissipation[28] and stiffness[29,30] have been explored by a new AFM technique, PeakForce Quantitative NanoMechanics (PF-QNM),[31] which provides simultaneous high resolution mapping of morphology and quantitative mechanical properties at the nano scale. However, the majority of the studies using PF-QNM are in the dry state and PF-QNM has been successfully used for the mapping of mechanical properties.[32–35] Nellist *et al.* have very recently shown the possibility of using PF-QNM for the simultaneous characterization of surface topography, quantitative nanomechanics, nanoelectronic properties, and electrochemical activity and peak force-scanning electron microscopy (PF-SECM) to probe the electrical conductivity of electrode surfaces in liquid.[35]

In the current study, the PF-QNM mode was used for the first time to study the interactions of charged species in a liquid medium and is considered highly challenging due to the liquid medium used as well as due to the nanosized materials and ionic species involved. Thus, the current study investigates the adsorption behavior of metal ions on TOCNF using different AFM modes in dry and aqueous media as well as SEM and spectroscopy in the dry state, taking Cu(II) as an example, which is one of the well-known toxic metals found in polluted water.[36] The adsorption process was first carried out in an *in situ* AFM study in a near-neutral liquid phase environment. The topography, adhesion and stiffness were selected and compared to study the physiochemical properties of TOCNF before and after adsorption in a close to neutral pH (100 mg L^{-1} $CuNO_3$ solution) using PF-QNM. In this work, we use the method to map differences by rapidly acquiring force distance curves between the tip and the same single nanofiber, which is a big challenge, particularly when the aqueous medium needs to be changed several times during measurements. TOCNF with adsorbed Cu(II) (TOCNF + Cu) under the studied pH were used for zeta-potential, topography and elemental studies. AFM images, SEM-EDS and XPS studies revealed a layer of copper and copper nanoparticles and confirmed the adsorption on the surface of the nanofibers. The structure change of the TOCNF because of the adsorption was further investigated by Raman and FTIR characterization at the molecular scale. The results show that this combination of techniques provides complimentary information on the metal ion adsorption and the techniques well supported each other to uncover the mysteries of the adsorption mechanism at the nano and molecular scales. This method can be employed to study the other types of cellulose with different functional groups for adsorption of any positively charged species and could be tailored for water purification in real contaminated water environments.

Results and discussion

In this study, we focused on using TOCNF with a high oxidization degree of carboxylate groups (1.2 mmol g^{-1}). The key design principle is to find evidence of the adsorption of Cu(II) onto the TOCNF in both aqueous and dry environments by *in situ* AFM and SEM measurements and further prove the adsorption by spectroscopy both at the nano and molecular scales.

The micrographs of the TOCNF characterized by SEM and AFM revealed some differences at the micro and nano scales. The samples for the SEM measurements were directly droplet-deposited and dried in air with high concentrations of TOCNF, while the samples for the AFM characterization were diluted and spin coated[37] on the substrate to obtain dispersed single nanofibers. The morphology observed *via* SEM (Fig. 1a) shows bundles of TOCNF, since the nanofibers are aggregated together during the drying process. However, the AFM images show a different topography (Fig. 1b and c). The chains of TOCNF are modified with $-COO^-$ groups, so it is easier to obtain well-individualized single fibers in a dilute solution because of the repulsive force.[14] Fig. 1b and c also present very small fragments and different size distributions of the fiber with fiber length ranging from tens of nm to several hundreds

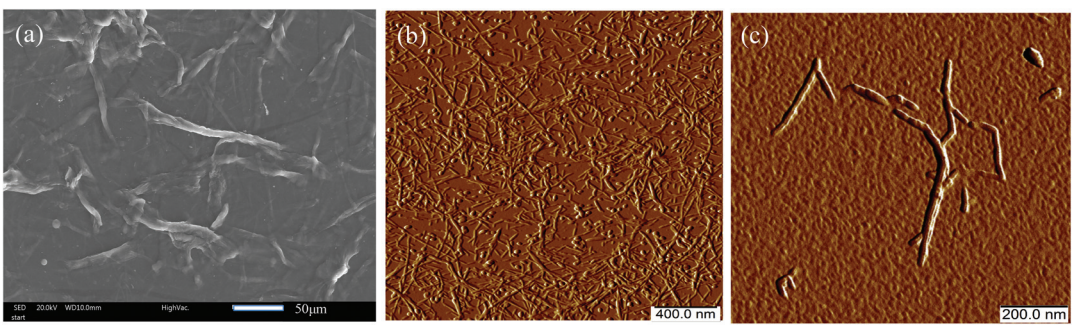

Fig. 1 SEM (a) and AFM peak force error images (b, c) of TOCNF.

of nm. This stems from the harsh modification process by the TEMPO method to obtain a high degree of oxidization for the TOCNF.

Zeta-potential measurements were performed at different pH values, adjusted using diluted nitric acid to study the colloidal stability and the surface charge of the TOCNF before and after the adsorption of Cu(II) (Fig. S1†). For the pure TOCNF, a range of zeta potentials between −43.3 and −64.8 mV were recorded, which confirmed the negative surface of the TOCNF and agreed with the data from our previous study.[19] After adding $CuSO_4$, all of the values of the zeta potentials under the studied pH values increased; for instance at pH 4.9 the zeta potential increased from −58.1 to −39.8. The trend of the zeta potentials of TOCNF + Cu agreed well with that of the TOCNF, indicating that the surface of the TOCNF had adsorbed positive Cu(II), leading to a less negative charged surface compared with that before adsorption. This is probably due to the fact that positively charged Cu(II) interact with the sorption sites (COO^- groups) on TOCNF and render TOCNF surfaces charge neutralized, resulting in a decrease in the negative surface charge and lower magnitude of the zeta-potential, depending on the availability of Cu(II).[19]

In situ AFM

Following the results of the zeta potential measurements, an *in situ* AFM study was carried out to study the adsorption behavior on a single TOCNF in aqueous medium. The detailed procedure is presented in the Materials and methods section. The morphology, adhesion and stiffness are discussed here. PF-QNM can acquire the topography image together with the individual force curves from each intermittent touch and analyze the instantaneous force on the tip, thus leading to the adhesion map. The stiffness of the single TOCNF at each pixel was extracted automatically by the software through the slope of the linear contact region from the retraction force curves[30] and could also be mapped simultaneously with high resolution.

The idea is to possibly identify the evidence for layers of Cu(II) or nanoparticles deposited on the surface of the fiber after adsorption, as reported previously.[13,19] Indeed, from the topography images, no layers or nanoparticles were observed clearly on the surface of the TOCNF + Cu (Fig. 2C). However, we found that the fiber ultimately shifts to the right, which is the same direction that the tip taps on the fiber, leaving the fingerprints of the fiber on the map (along the arrow in Fig. 2C). Mainly, the shifting is ascribed to the constant tapping by the tip during the measurements because the TOCNF swell easily in a liquid and become softer.[38]

(3-Aminopropyl)triethoxysilane (APTES) is positively charged and was employed to anchor the fiber by a vapor-phase method[39] because the TOCNF has very good hydrophilicity in solution and is easily displaced or lost during measurement in the liquid because the tip continuously taps the fiber at a high frequency (2 kHz). The surface charge of the tip used for AFM measurements is negative, so theoretically, there will be only a repulsion force between the TOCNF or TOCNF + Cu and the probe because the TOCNF and TOCNF + Cu are also negatively charged based on the zeta-potential study.

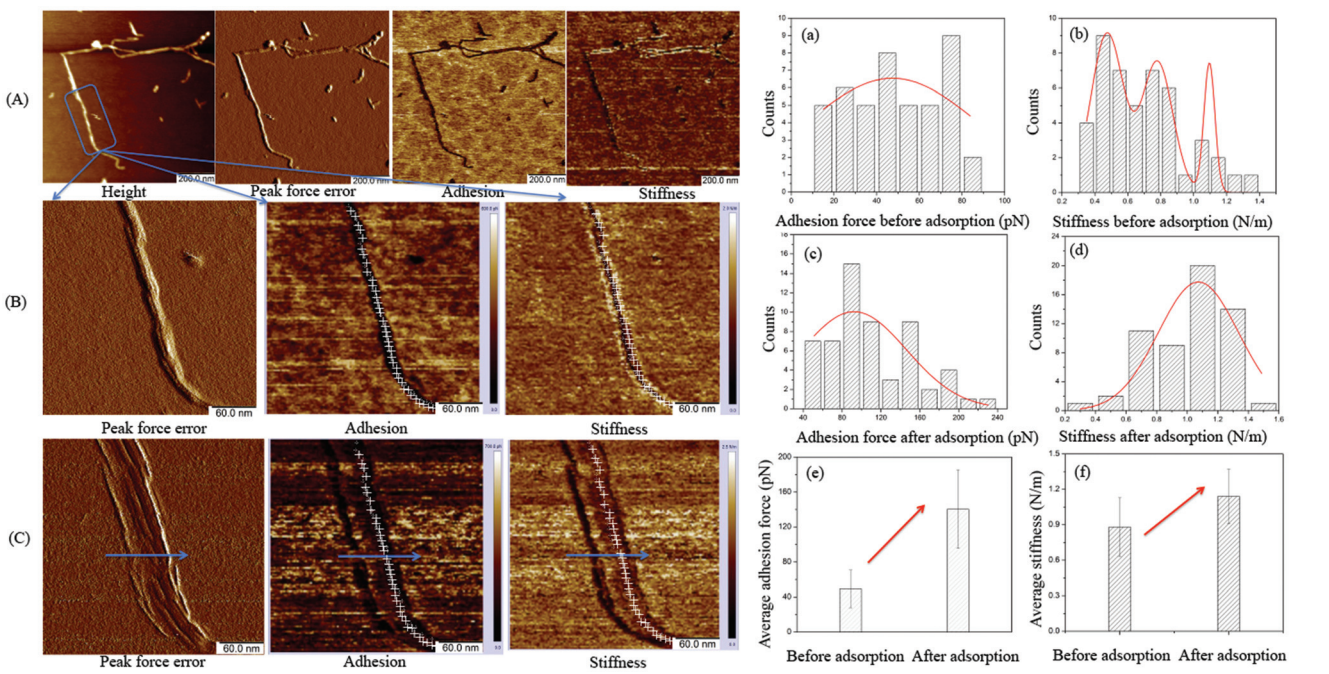

Fig. 2 Height, peak force error, adhesion and stiffness images of TOCNF obtained by the PF-QNM mode before (A, B) and after adsorption (C) with Cu(II); the corresponding histogram of the distribution of adhesion and stiffness along the fiber before (a, b) and after (c, d) Cu(II) adsorption with the average values shown in e and f.

However, the adhesion map still shows very little adhesion force along the fiber before the Cu(II) adsorption (Fig. 2A and B). This might come from the interaction between the negatively charged tip and positively charged APTES. The color of the adhesion force along the fiber is black, which means that the adhesion force is much smaller compared with the adhesion force on the APTES (the brown blank area) because the fiber is lying between APTES and the tip, preventing the interaction between the APTES and the tip.

Fig. 2B and C show the adhesion and stiffness images of the single TOCNF obtained from a series of force curves before and after the adsorption of Cu(II). In the images, the darker the region is, the smaller the value is. It is hard to analyze the changes in the physiochemical properties based on the maps. Therefore, the data on every pixel along the fiber (white cross) were used to evaluate the adhesion and stiffness distribution on that individual TOCNF and fitted with Gaussian curves. The average values of adhesion force and stiffness before and after adsorption were calculated (Fig. 2a–f). It could be clearly seen that the average adhesion force increased from 50 pN to 140 pN (Fig. 2e), which is due to the interaction between the positive Cu(II) and the negative tip after Cu(II) binding on the $-COO^-$ groups of the fiber, which increased the electrostatic force. The stiffness was also enhanced from 0.87 N m^{-1} to 1.13 N m^{-1} (Fig. 2f), which revealed that the adsorbed Cu(II) covered the surface and hardened the fiber. The physiochemical properties like adhesion and stiffness can be characterized by PF-QNM measurements not only qualitatively but also quantitatively. Despite its many advantages, it should be noted that the described experimental method in the current work is more qualitative than quantitative, due to its complexity and multi-step calibration procedure. Even if done properly, the calibration may not produce fully correct (quantitative) results, especially if the model used by the AFM designer is not appropriate.[31,40]

Therefore, although no direct evidence of Cu adsorption on a single TOCNF was visualized by the AFM imaging in liquid, the adsorption process was still proved by the enhancement of the adhesion and stiffness from PF-QNM measurements. With careful control of the operating parameters, the physiochemical properties measured under different environmental conditions could shed light on the study of the adsorption behavior at the nano scale.

Following the above measurements in liquid, the TOCNF after adsorption with Cu(II) (TOCNF + Cu) at pH 6.7 were used for further characterization because TOCNF show the best adsorption capacity under near-neutral pH conditions.[12,19] The TOCNF–Cu solution was droplet-deposited and measured in dry form by AFM. Fig. 3 shows the AFM amplitude error images of TOCNF + Cu and the corresponding 3D height images (a–f).

Fig. 3a shows bundles of TOCNF + Cu, which agrees with the SEM images of the raw material in Fig. 1. Fig. 3b corresponds to the blue square area in Fig. 3a. Fig. 3c–f shows the blue square area in Fig. 3b. A nanoparticle approximately 100 nm in diameter on top of the fibers is clearly shown in Fig. 3c, which agrees with our previous study.[19] Nanoparticles from approximately 10 to 100 nm in diameter were also discovered in the blue circle area from Fig. 3d. Fig. 3e shows a layer of nanofibers on the flat area of the big bundle of fibers in Fig. 3b. Between the single nanofibers, small valleys could be found and are more clearly shown in Fig. 3f. However, the surface of the TOCNF before adsorption (Fig. 3g, R_a = 3.8 nm) is much smoother (filled valleys) compared with TOCNF + Cu (Fig. 3e, R_a = 8.9 nm). This means that, apart from the copper nanoparticles, Cu(II) was adsorbed on the surface of single TOCNF and formed a layer of copper that covered the nanofibers. This was further confirmed by studying the adsorption of Cu ions onto TOCNF at different $CuSO_4$ concentrations.

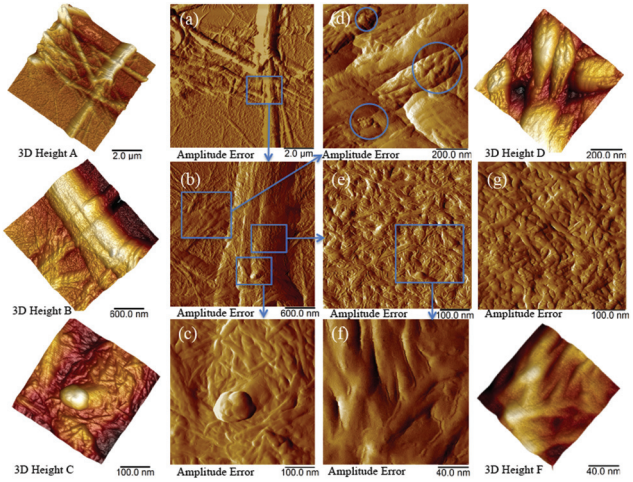

Fig. 3 The AFM amplitude error images of TOCNF + Cu and the corresponding 3D height images (a–f). A shows bundles of TOCNF + Cu; b shows the blue square area in a; c, d, e, and f show the blue square area in b; g shows the AFM amplitude error image of TOCNF (without adsorption).

Fig. 4 shows that the size of the copper nanoparticles increased with the addition of $CuSO_4$. Around 100–200 nm, copper nanoparticles could be clearly seen from Fig. 4a, while TOCNF adsorbed in 50 mg L^{-1} $CuSO_4$ shows that the size of the copper nanoparticles is less than 50 nm (Fig. 1b). When the $CuSO_4$ solution concentration is lower than 30 mg L^{-1}, no copper nanoparticles could be seen from the AFM images, but a nanolayer of copper covered the TOCNF surface. This confirms that TOCNF adsorption could happen within the range of $CuSO_4$ solution in this work and the clustering into nanoparticles occurs only above a given threshold concentration of metal ions.

Spectroscopic validation

We further confirmed the presence of the elements on the fiber after adsorption by SEM-EDS measurements. Copper nanoparticles (NPs) were found on the fiber, which are probably formed by the Cu(II) adsorbed by carboxylate groups on the surface of the cellulose nanofibers as well as self-assembly, micro-precipitation and oxidation in dry form (Fig. 5a, b and f),[19]

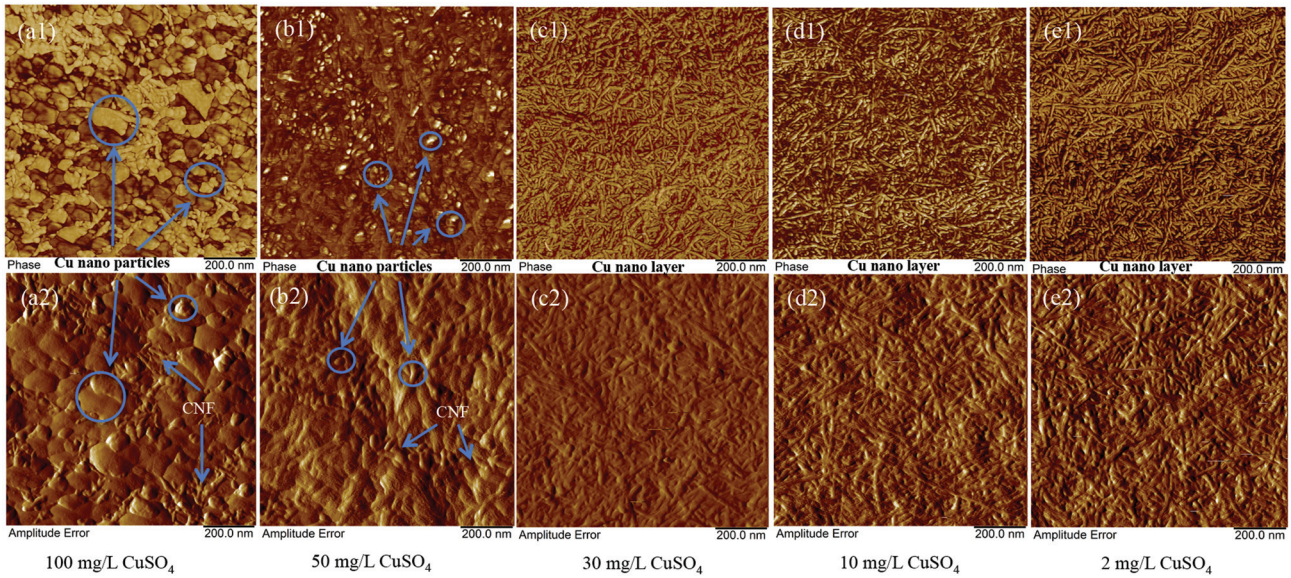

Fig. 4 AFM morphology of the adsorption of Cu ions onto TOCNF 1.2 at different concentrations of $CuSO_4$ solution.

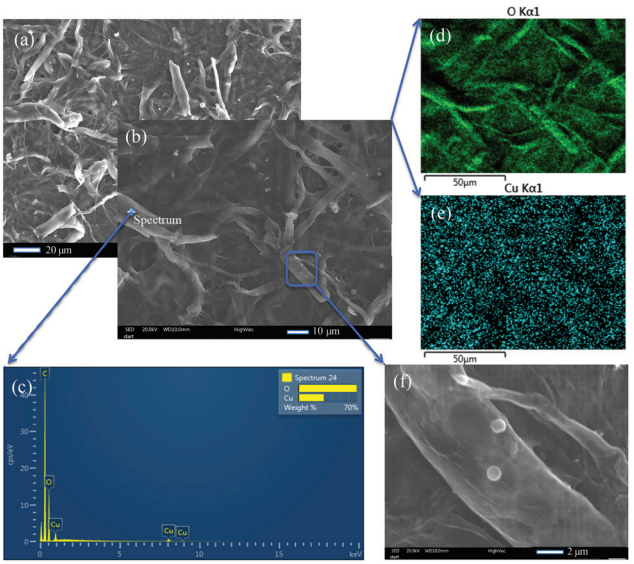

Fig. 5 SEM images (a, b, f) and SEM-EDS maps (d, e) of dried TOCNF + Cu; c is the EDS spectrum taken on the fiber surface from the spot in image b; d and e are the oxygen and copper EDS maps, respectively.

but no nanoparticles could be found on the surface before the copper adsorption. Apart from the NPs, the spectrum on the cellulose also indicated that Cu(II) was adsorbed on the surface of the cellulose nanofibers (Fig. 5b and c). The green oxygen EDS map (Fig. 5d) gives the same skeleton of the TOCNF as the SEM image in Fig. 5b. The blue dots on the EDS map (Fig. 5e), which stand for the detected copper, clearly covered both the fiber and nanoparticle regions.

Moreover, the EDS maps show more evidence that the copper was homogenously adsorbed on the surface of the TOCNF, which is consistent with the AFM findings. The form of the copper nanoparticles was further studied by XPS measurements. Apart from the C 1s and O 1s peaks for both samples, the TOCNF before adsorption also shows a Na 1s peak at 1071.7 eV (Fig. 6a and c), which comes from the TEMPO oxidation process.[14] After adsorption, different sates of Cu including Cu(I) and Cu(II) show up between 930–965 eV.[41,42] For Cu $2p_{3/2}$, 1.7% of Cu(II) at 935.2 eV and 0.8% of Cu(I) at 933.1 eV were found in the sample TOCNF + Cu (Fig. 6b and c). Obviously, Cu(II) comes from the $CuSO_4$ solution during the adsorption process. Cu(II) could also be reduced by the aldehyde group which partly exists in TOCNF samples[14] and finally leads to Cu(I). Then Cu(I) and Cu(II) followed with self-assembly/micro-precipitation and oxidation and led to the copper nano-layer and nanoparticles on the surface of TOCNF. The other states of copper like Cu $2p_{1/2}$ are also shown in Fig. 6b,[43] and confirmed the above states of copper, but are not discussed here because of their low concentration (less than 0.5%).

Raman and IR spectroscopy proved to be useful methods to study the mechanisms of divalent copper binding to a modified cellulose adsorbent.[44] In the current study, wood cellulose and the corresponding TEMPO modified nanofibers with two degrees of oxidation (TOCNF 0.6 and TOCNF 1.2) were used to define the relevant peaks responsible for adsorption. Since copper nanoparticles could screen the Raman spectra of TOCNF + Cu and lead to a significant fluorescence effect, only 2 mg L^{-1} $CuSO_4$ solution was adsorbed on wood cellulose, TOCNF 0.6 and TOCNF 1.2 used for the Raman study, to obtain good spectra without the fluorescence effect. Meanwhile, samples of wood cellulose, TOCNF 0.6 and TOCNF 1.2 after adsorption in 100 mg L^{-1} $CuSO_4$ solution were used for FTIR characterization.

Typical Raman spectra of the raw materials wood cellulose and TEMPO oxidized wood cellulose TOCNF 0.6 and TOCNF

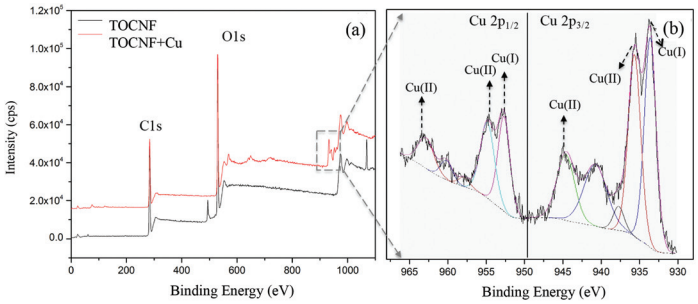

(c)

	TOCNF		TOCNF+Cu		
	BE. eV	AC. atom.%	BE. eV	AC. atom.%	
C 1s	285.0	18.46	285.0	13.07	C-(C.H)
	286.6	33.69	286.6	32.24	C-OH
	288.2	11.77	288.2	12.88	O-C-O
	289.3	0.47	289.4	2.03	COOH
O 1s	531.3	3.31	531.6	1.28	Na-O/ C=O
	533.1	30.36	532.9	36	C-OH
Na 1s	1071.7	1.95			Na(I)
Cu $2p_{3/2}$			933.1	0.84	Cu(I)
			935.2	1.67	Cu(II)

Fig. 6 XPS survey spectra of TOCNF (before adsorption) and TOCNF + Cu (after adsorption); binding energy (BE) and atomic concentration (AC) of the elements according to the XPS spectrum values of TOCNF and TOCNF + Cu.

1.2 before and after exposure to a $CuSO_4$ suspension are shown in Fig. 7. Most of the observed Raman peaks are ascribed to vibrations of the cellulose backbone between 800 and 1500 cm^{-1}. Fig. 7(a) shows very clear peaks around 1590–1595 cm^{-1} for the above three materials. By careful assignment, the peak at 1595 cm^{-1} belongs to lignin from wood cellulose.[45,46] After TEMPO modification, the peak at 1590 cm^{-1} almost doubled in intensity for TOCNF 1.2 compared to TOCNF 0.6 (see Fig. S2†). This confirms the position of the peak introduced due to TEMPO oxidation and is assigned to the vibration of C=O bonds on the carboxylate group.

After Cu(II) adsorption, the peak at 1590 cm^{-1} for TOCNF 0.6 and TEMPO 1.2 almost vanishes in Fig. 7(b). This might be a consequence of Cu(II) adsorption with subsequent reduction to Cu(0) and the screening of the adsorption sites – carboxylate groups. After Cu adsorption the intensity of the 1595 cm^{-1} peak decreased for wood cellulose to about half the initial intensity. The reason might be that the lignin was also partly adsorbed Cu(II) onto its –COOH function groups and thereby affected the C=O vibration. Very low intensity peaks around 1595 cm^{-1} could also be found in TOCNF 0.6 and TEMPO 1.2 samples after adsorption, indicating some residual lignin in the TEMPO oxidised nanofibers. But these small intensity peaks are overlapped by the strong peak of COO^- groups before adsorption, Fig. 7(a). Thus a clear decrease in intensity of the peaks around 1590–1595 cm^{-1} was noted for all the materials (Fig. S2†) and the magnitude of the decrease in intensity agrees with the expected adsorption. Another interesting peak appears at 2545 cm^{-1} together with some noise spectrum around 2000–2400 cm^{-1}, which is unknown for us and needs to be studied further in the future.

In parallel, FTIR was employed to access the changes in the vibrational properties of the TOCNF caused by adsorption of Cu(II). Fig. 8 shows the FTIR spectra of the wood cellulose and TOCNF (0.6, 1.2 mmol g^{-1}), which exhibit characteristic bands of cellulose.[47] As compared with the spectrum of unmodified wood cellulose, the characteristic vibrations of the carboxylate moieties were easily detected in the spectra of TOCNF samples, which are at 1404 cm^{-1} ($\nu_s COO^-$) and 1597 cm^{-1} ($\nu_{as} COO^-$).[13] The intensity of these bands progressively increased with the DO and shifted to lower wavenumbers due to a higher amount of C=O (Fig. 8c).

After adsorption, the intensity of the $\nu_s COO^-$ band at 1597 cm^{-1} and 1599 cm^{-1} decreased and shifted to 1600 cm^{-1} and 1602 cm^{-1} for TOCNF 1.2 and TOCNF 0.6, respectively (Fig. 8d). This is because that part of the C=O bond binds with Cu(II) and leads to the decrease of intensity and band shift. But the $\nu_s COO^-$ band at 1635 cm^{-1} doesn't change after adsorption in both band position and intensity, which means that no significant adsorption happened for wood cellulose. No band position change of $\nu_{as} COO^-$ at 1404 cm^{-1} to 1427 cm^{-1} for all of the materials could be found after adsorp-

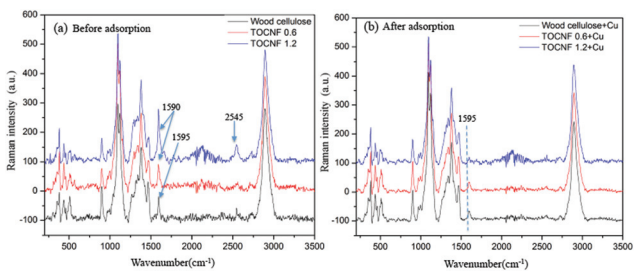

Fig. 7 Raman spectra of wood cellulose, TOCNF (0.6, 1.2 mmol g^{-1}), before and after adsorption in 2 mg L^{-1} $CuSO_4$ solution.

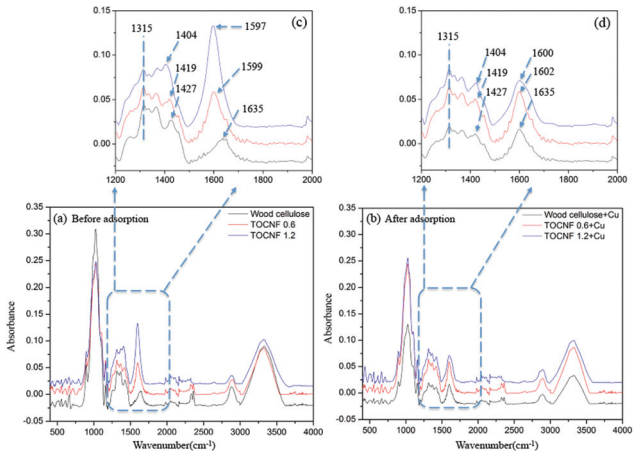

Fig. 8 FTIR spectra of wood cellulose, TOCNF 0.6, TOCNF 1.2 (before adsorption), and wood cellulose + Cu, TOCNF 0.6 + Cu, TOCNF 1.2 + Cu (after adsorption).

tion, but the intensity of these bands slightly decreased due to adsorption (Fig. 8d). These results give further supporting evidence of the binding interaction of copper ions with the carboxylate groups on the TOCNF during the adsorption process.

In general, it is considered that the "affinity" or "adsorption" between the COO^- group and Cu(II)[48] may be driven by one or a combination of processes such as ion exchange, complexation, coordination, adsorption, electrostatic interaction, chelation and covalent bonding. It was not possible to clearly define the nature of interaction in the current system from the AFM or spectroscopic data. The binding energies and bond lengths of carboxylate cellulose nanofibrils (CNFs) and different types of metal ions were calculated by Williams *et al.*[49] This group found that electrostatic interactions dominate the bonding between the cellulose nanofibril system and an alkali, alkaline earth or main group cation, as opposed to transition metal cations that could form a stronger covalent bond with the CNFs.

Fig. 9 shows a schematic representation of the probable mechanism of copper ion adsorption on TOCNF from aqueous to dry states based on the experimental studies. In a liquid medium, the carboxyl groups have a resonance stabilized structure with an electronic cloud between both C–O bonds with 1 negative charge in between (Fig. S3, II†). Due to the "affinity" between the COO^- groups and the positively charged Cu(II), charge neutralization occurs and forms less negatively charged TOCNF (Fig. 9, step 1). During the interaction, most Cu(II) receive electrons from one COO^- and form into $-COO^-Cu$. Part of the Cu(II) could be reduced to Cu(I) by the aldehyde group. Thereafter self-assembly/micro-precipitation of $-COO^-Cu$ and oxidation of Cu(I) to Cu(II) in air (Fig. 9, step 2) will convert Cu(I) and/or Cu(II) into copper oxide nanolayers or nanoparticles, which was proved by XPS and AFM measurements. Our earlier study on the DFT modelling of Ag ions on functionalized cellulose also suggested that the attachment of multiple ions on a functional site is energetically favourable and supports the cluster formation.[10] However, we do not have any indication of the clustering in liquid medium and the concentration threshold for clustering in liquid phase. This can be the topic for further research and can also be supported by modeling studies.

Experimental section

Materials

TEMPO-oxidized cellulose nanofibers (TOCNF) (1.2 mmol g^{-1}) were kindly provided by EMPA, Switzerland. Copper(II) sulfate pentahydrate, sodium hydroxide, nitric acid, and (3-aminopropyl)triethoxysilane (APTES) were all obtained from Sigma-Aldrich and used as received. Degassed Milli-Q water was used as a solvent and as a reference liquid in AFM measurements.

In situ adsorption study by AFM

AFM sample preparation. The AFM metal disc was glued by freshly cleaved mica and coated with APTES using the vapor-phase method.[38] 0.01 wt% TOCNF was spin-coated on the surface-modified metal disc to obtain separate single nanofibers.[36]

In situ PeakForce QNM measurements

A FastScan AFM (Bruker, NanoScope V controller, Santa Barbara, California, USA) with the PF-QNM mode was used for the *in situ* study. Standard ScanAsyst-Fluid+ silicon nitride tips (Bruker, USA) with the spring constant k = 0.70 ± 0.05 N m^{-1} (determined by the thermal tune method using the built-in option in the AFM software NanoScope 9.1) and a tip radius of 2 nm were used and treated with a UV Ozone Cleaner (ProCleaner™ Plus, USA) for 20 minutes beforehand. The spring constant was carefully measured before and after experiments and kept a constant. The *in situ* adsorption process by AFM is described as follows: (1) the sample was mounted on the scanner; the sample and the tip were covered by drops of degassed Milli-Q water; the morphology, adhesion force and stiffness were first measured in MQ water; (2) MQ water was removed and 100 mg L^{-1} $CuSO_4$ solution was added for 5 minutes to ensure adsorption; (3) the $CuSO_4$ solution was

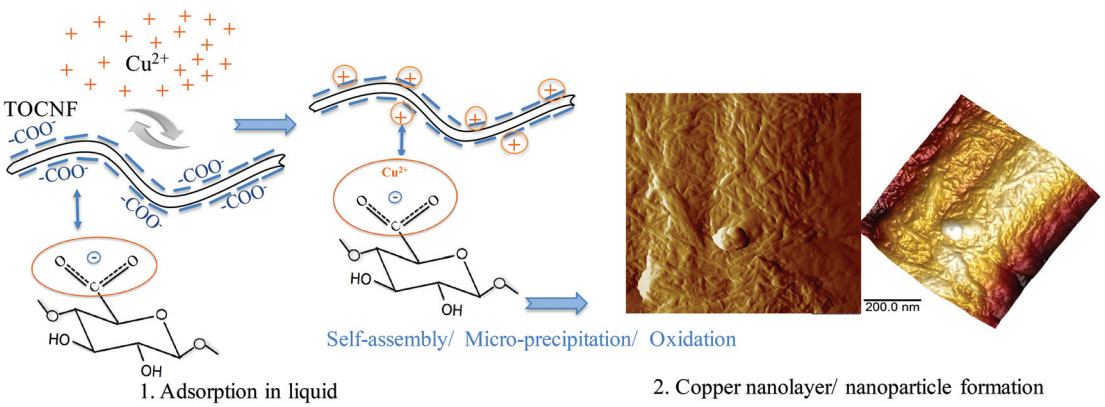

Fig. 9 Scheme showing the mechanism of copper ion adsorption on TOCNF from the aqueous to the dry state. Step 1 is the adsorption between TOCNF and Cu(II) in liquid. The equilibrium structure of the TOCNF unit is shown in Fig. S4 (II).† Step 2 (AFM images) shows the oxidation process of copper in air and formation of copper nano-layers and nanoparticles after self-assembly/micro-precipitation.

exchanged and rinsed thrice with MQ water; (4) the sample was scanned on the same fiber in fresh MQ water as described in step (1). Great attention must be paid here while exchanging the liquid to make sure that the sample is not touched, which would lose the fiber. The liquid was exchanged within 10 seconds, so that the fiber does not dry during the above steps. All experiments were performed at room temperature. The fast scan machine was totally covered by a hood during measurements to prevent the evaporation of the liquid. The measurements were operated in the PeakForce QNM mode in liquid using the NanoScope 9.1 software. The peak force was set at 1 nN by carefully adjusting the peak force set point values, since high peak forces would deform the material, but very low peak forces could not provide stable images and mechanical properties. The minimum peak force could obtain a stable morphology of the fibers and was also useful for the calculation of the mechanical properties.[30] The scan rate was set at 1.0 Hz. All of the measurements were done by oscillating the sample in the normal direction with a frequency of 2 kHz while scanning the sample in the lateral direction. The morphology, adhesion force and stiffness before and after adsorption on the same single fiber were investigated under the same setup. Three parallel experiments using new probes and new samples within one setup were performed. The experiments gave reproducible results, and a representative image was selected for the discussion section. The collected data along the fiber (totally around 50–60 values) were processed with NanoScope Analysis 1.5 (Bruker) and fitted with a Gaussian curve, which gives rise to the average value of the adhesion force and stiffness.

Fabrication of TOCNF adsorbed with Cu(II)

100 mg L^{-1} $CuSO_4$ solutions at different pH values (3.0, 4.1, 4.9, 5.7, 6.9) were prepared from $CuSO_4{\cdot}5H_2O$ and used for TOCNF adsorption. 100 mg L^{-1}, 50 mg L^{-1}, 30 mg L^{-1}, 10 mg L^{-1} and 2 mg L^{-1} $CuSO_4$ solutions at pH 5.7 were also prepared from $CuSO_4{\cdot}5H_2O$ and used for spectroscopy studies. All experiments for copper adsorption were performed at a dosage of 0.5 g L^{-1} of TOCNF with a volume of 50 mL. The samples (TOCNF + Cu) were then filtered and washed with distilled water with a membrane pore size of 0.45 μm (DVPP, Millipore).[19] TOCNF + Cu were collected on the filter membranes and used for analysis by AFM measurements, zeta sizing, SEM-EDS, Raman and ATR-FTIR.

Characterization

Zeta potential. The zeta potential of the TOCNF and TOCNF + Cu at different pH values (3.0, 4.1, 4.9, 5.7, 6.9) and at a concentration of 0.05 wt% was measured using a Zetasizer Nano ZS, Malvern (UK) at 25 °C. TOCNF was first treated with $CuSO_4$, and then filtered and washed with distilled water to remove the free ionic $CuSO_4$. Thereafter, TOCNF with adsorbed Cu(II) were diluted in a nitric acid solution to different pH values for zeta potential measurements. The same amount of TOCNF without adsorption was also diluted in the same pH nitric acid solution for zeta potential measurements, which is used as the control.

Atomic force microscopy (AFM). The morphology of the samples with and without copper adsorption was determined with a MultiMode 8 AFM (Bruker, NanoScope controller, Santa Barbara, California, USA). The TOCNF and TOCNF + Cu solution were drop coated on the metal pug substrate and dried in air before being measured. The height, amplitude and phase images were recorded using the probe (Model: TESPA-V2, Bruker) under tapping mode. The collected data were processed with the software NanoScope Analysis 1.5 (Bruker).

Scanning electron microscopy-energy dispersive X-ray spectroscopy (SEM-EDS). The morphology of the samples with and without copper adsorption was also observed using scanning electron microscopy (JEOL IT300, Japan). The samples were placed on conductive tape and sputter coated with carbon. Images were taken operating at 2.5 kV and 10 mm working distance was used for Energy Dispersive X-ray Spectroscopy measurements. Spot and map profiles showed the elemental distribution in the sample surface.

X-ray photoelectron spectroscopy (XPS). XPS was used to determine the surface elements after adsorption. All XPS spectra were collected using an Axis Ultra DLD electron spectrometer (Kratos Analytical Ltd, UK) using a monochromatic Al K_α source operated at 150 W and an analyser pass energy of 160 eV for acquiring wide spectra and a pass energy of 20 eV for individual photoelectron lines. The surface potential was stabilized by the spectrometer charge neutralization system. The binding energy (BE) scale was referenced to the C 1s line of aliphatic carbon, set at 285 eV. Processing of the spectra was accomplished using the Kratos software.

Raman spectroscopy. The wood cellulose, TOCNF 0.6 and TOCNF 1.2 were first adsorbed in 2 mg L^{-1} $CuSO_4$ solution, followed by filtration and washing with distilled water to remove the unadsorbed Cu(II). All of the above materials were vacuum dried at 50 °C for 6 hours and used for Raman measurements. Raman characterization of the cellulose material was conducted using a CRM 200 confocal Raman microscope (Witec), equipped with a 2.33 eV excitation laser. The spectra were recorded at 6 cm^{-1} resolution using a ×100 objective at a power of 5.8 mW measured directly on the sample stage of the microscope. Special care was taken to avoid sample overheating from the laser beam. To take into account possible sample inhomogeneity, the spectra were collected from 20 randomly chosen points on each sample surface with subsequent averaging. All the presented Raman spectra were baseline corrected *via* subtraction of fluorescence background and normalized by the peak at 1095 (cm^{-1}).

Attenuated total reflection-Fourier transform infrared spectroscopy (ATR-FTIR). The wood cellulose, TOCNF 0.6 and TOCNF 1.2 were first adsorbed in 100 mg L^{-1} $CuSO_4$ solution, followed by filtration and washing with distilled water to remove the unadsorbed Cu(II). All of the above materials were vacuum dried at 50 °C for 6 hours and used for FTIR measurements. The infrared spectra were recorded at room temperature (~23 °C) with a resolution of 2 cm^{-1} on a Bruker Vertex 80 V FTIR instrument equipped with a DLaTGS detector and a

mid-infrared excitation source using the Platinum Attenuated Total Reflection accessory with a single reflection diamond crystal. Both the optical bench and the sample chamber were under vacuum (1.9 hPa) for each measurement. All measurements were repeated at least twice to assure good spectral averaging. The presented ATR-FTIR spectra were baseline corrected *via* subtraction of fluorescence background and normalized by the peak at 1028 cm^{-1}.

Conclusions

In summary, the adsorption behavior between the TEMPO-mediated oxidation nanofibers and Cu(II) was investigated at the nano and molecular scales in this study. The PF-QNM mode provides both quantitative and qualitative characterization methods and was demonstrated to be very helpful for studying the surface interaction and adsorption behavior between the metal ions and the functionalized nanofibers in the liquid phase by *in situ* AFM study. The AFM, SEM-EDS and XPS results agreed with each other and were further supported by extensive spectroscopic characterization. This methodology can be successfully extended to understand the interaction of cellulose nanofibers or nanocrystals with other charged species in water.

All the results indicate that Cu(II) was first adsorbed by the carboxylate groups grafted on cellulose chains in aqueous medium followed by the copper nano-layer/nanocluster formation process, during drying in air. Apart from water purification, numerous applications could be developed based on the conductivity properties of nanocellulose adsorbed with metal ions *viz*. cellulose nanopaper and film for opto-electronics,[50,51] electrochemical electrodes,[52] flexible supercapacitors and transistors,[53,54] nanocomposites[55] and other electrical devices[56] and will be included along with other subjects in our future work plan. However, the self-assembly/clustering of Cu in liquid medium has not been confirmed or evaluated, which will be of interest in future works.

Acknowledgements

The authors gratefully acknowledge financial support from the Swedish Research Council (VR, grant no. 621-2013-5997) and FORMAS (Eranet SUSFOOD, CEREAL project; no. 222-2014-18). We thank Liu, P. and Naseri, N. of Luleå University of Technology, Sweden for their assistance with the zeta potential and ATR-FTIR studies, respectively. Zhu, C. is especially grateful to Fielden, M. of the Royal Institute of Technology (KTH), Sweden for his technical support in PeakForce QNM measurements.

Notes and references

1 M. A. Hubbe, J. Park and S. Park, *BioResources*, 2014, **9**, 7782–7925.
2 N. Lin, J. Huang and A. Dufresne, *Nanoscale*, 2012, **4**, 3274–3294.
3 D. Klemm, B. Heublein, H. Fink and A. Bohn, *Angew. Chem., Int. Ed.*, 2005, **44**, 3358–3393.
4 B. Volesky, *Water Res.*, 2007, **41**, 4017–4029.
5 J. Crédou and T. Berthelot, *J. Mater. Chem. B*, 2014, **2**, 4767–4788.
6 H. Ma, C. Burger, B. S. Hsiao and B. Chu, *Biomacromolecules*, 2012, **13**, 180–186.
7 Z. Karim, A. P. Mathew, M. Grahn, J. Mouzon and K. Oksman, *Carbohydr. Polym.*, 2014, **112**, 668–676.
8 C. Zhang, R. Z. Zhang, Y. Q. Ma, W. B. Guan, X. L. Wu, H. Liu, Y. L. Du and C. P. Pan, *ACS Sustainable Chem. Eng.*, 2015, **3**, 396–405.
9 A. Sato, R. Wang, H. Ma, B. S. Hsiao and B. Chu, *J. Electron Microsc.*, 2011, **60**, 201–209.
10 C. Zhu, I. Dobryden, J. Ryden, S. Öberg, A. Holmgren and A. P. Mathew, *Langmuir*, 2015, **31**, 12390–12400.
11 H. Ma, B. S. Hsiao and B. Chu, *ACS Macro Lett.*, 2012, **1**, 213–216.
12 P. Liu, P. F. Borrell, M. Božic, V. Kokol, K. Oksman and A. P. Mathew, *J. Hazard. Mater.*, 2015, **294**, 177–185.
13 H. Sehaqui, U. P. Larraya, P. Liu, N. Pfenninger, A. P. Mathew, T. Zimmermann and P. Tingaut, *Cellulose*, 2014, **21**, 2831–2844.
14 A. Isogai, T. Saito and H. Fukuzumi, *Nanoscale*, 2011, **3**, 71–85.
15 S. Ifuku, M. Tsuji, M. Morimoto, H. Saimoto and H. Yano, *Biomacromolecules*, 2009, **10**, 2714–2717.
16 H. Liu, D. Wang, Z. Song and S. Shang, *Cellulose*, 2011, **18**, 67–74.
17 S. Zhang, B. Sun, W. Wang, M. Zhu and J. Chen, *J. Macromol. Sci., Part A: Pure Appl. Chem.*, 2006, **43**, 1895–1906.
18 T. Saito and A. Isogai, *Carbohydr. Polym.*, 2005, **61**, 183–190.
19 P. Liu, K. Oksman and A. P. Mathew, *J. Colloid Interface Sci.*, 2016, **464**, 175–182.
20 E. A. Sosnov, S. A. Belova and A. A. Malygin, *Semiconductors*, 2007, **41**, 495–497.
21 H. A. Harms, N. Tétreault, K. Voïtchovsky, F. Stellacci and M. Grätzel, *Phys. Chem. Chem. Phys.*, 2012, **14**, 9037–9040.
22 T. Yamada and S. Shiratori, *Electr. Eng. Jpn.*, 2002, **141**, 1–7.
23 A. Beaussart, A. Mierczynska-Vasilev and D. A. Beattie, *J. Colloid Interface Sci.*, 2010, **346**, 303–310.
24 P. R. P. Paiva, M. B. M. Monte, R. A. Simão and J. C. Gaspar, *Miner. Eng.*, 2011, **24**, 387–395.
25 N. Nordgren, P. Eronen, M. Österberg, J. Laine and M. W. Rutland, *Biomacromolecules*, 2009, **10**, 645–650.
26 M. Eliyahu, S. Emmanuel, R. J. Day-Stirrat and C. I. Macaulay, *Mar. Pet. Geol.*, 2015, **59**, 294–304.
27 T. J. Young, M. A. Monclus, T. L. Burnett, W. R. Broughton, S. L. Ogin and P. A. Smith, *Meas. Sci. Technol.*, 2011, **22**, 125703.
28 A. Chlanda, J. Rebis, E. Kijenska, M. J. Wozniak, K. Rozniatowski, W. Swieszkowski and K. J. Kurzydlowski, *Micron*, 2015, **72**, 1–7.

29 B. Zhao, X. Wang, Y. Song, J. Hu, J. Lü, X. Zhou, R. Tai, X. Zhang and L. Zhang, *Phys. Chem. Chem. Phys.*, 2015, **17**, 13598–13605.
30 B. Zhao, Y. Song, S. Wang, B. Dai, L. Zhang, Y. Dong, J. Lü and J. Hu, *Soft Matter*, 2013, **9**, 8837–8843.
31 M. E. Dokukin and I. Sokolov, *Langmuir*, 2012, **28**, 16060–16071.
32 G. Smolyakov, S. Pruvost, L. Cardoso, B. Alonso, E. Belamie and J. Duchet-Rumeau, *Carbohydr. Polym.*, 2016, **151**, 373–380.
33 H. Schillers, I. Medalsy, S. Hu, A. L. Slade and J. E. Shaw, *J. Mol. Recognit.*, 2016, **29**, 95–101.
34 W. Wang, Z. Guo, J. Sun and Z. Li, *Biopolymers*, 2017, **107**, 61–69.
35 M. R. Nellist, Y. Chen, A. Mark, S. Gödrich, C. Stelling, J. Jiang, R. Poddar, C. Li, R. Kumar, G. Papastavrou, M. Retsch, B. S. Brunschwig, Z. Huang, C. Xiang and S. W. Boettcher, *Nanotechnology*, 2017, **28**, 095711–095729.
36 A. K. Shrivastava, *J. Environ. Prot.*, 2009, **29**, 552–560.
37 M. A. Herrera, A. P. Mathew and K. Oksman, *Carbohydr. Polym.*, 2014, **112**, 494–501.
38 K. Takada, D. J. Díaz, H. D. Abruña, I. Cuadrado, C. Casado, B. Alonso, M. Morán and J. Losada, *J. Am. Chem. Soc.*, 1997, **119**, 10763–10773.
39 M. Zhu, M. Z. Lerum and W. Chen, *Langmuir*, 2012, **28**, 416–423.
40 K. K. M. Sweers, K. O. Van Der Werf, M. L. Bennink and V. Subramaniam, *ACS Nano*, 2012, **6**, 5952–5960.
41 F. Klein, R. Pinedo, P. Hering, A. Polity, J. Janet and P. Adelhelm, *J. Phys. Chem. C*, 2016, **120**(3), 1400–1414.
42 R. Bendi and T. Imae, *RSC Adv.*, 2013, **3**, 16279–16282.
43 A. M. Salvi, F. Langerame, A. Macchia and M. L. Tabasso, *Chem. Cent. J.*, 2012, **6**(Suppl 2), S10.
44 D. W. O'Connell, B. Aszalos, C. Birkinshaw and T. F. O'Dwyer, *J. Appl. Polym. Sci.*, 2010, **116**, 2496–2503.
45 J. Ma, X. Zhang, X. Zhou and F. Xu, *BioEnergy Res.*, 2014, **7**, 1358–1368.
46 T. Röder and H. Sixta, *Macromol. Symp.*, 2005, **223**, 57–66.
47 S. Y. Oh, D. I. Yoo, Y. Shin and G. Seo, *Carbohydr. Res.*, 2005, **340**, 417–428.
48 J. Wang and C. Chen, *Biotechnol. Adv.*, 2009, **27**, 195–226.
49 K. S. Williams, J. W. Andzelm, H. Dong and J. F. Snyder, *Cellulose*, 2014, **21**, 1091–1101.
50 K. Mathew, K. Sundararaman, K. W. Weaver, T. A. Arias and R. G. Hennig, *J. Chem. Phys.*, 2014, **140**, 084106.
51 J. Chen, J. Xu, K. Wang, X. Qian and R. Sun, *ACS Appl. Mater. Interfaces*, 2015, **7**, 15641–15648.
52 Z. Liu, X. Wang, M. Li and W. Wu, *Nanotechnology*, 2015, **26**, 465708.
53 J. Huang, H. Zhu, Y. Chen, C. Preston, K. Rohrbach, J. Cumings and L. Hu, *ACS Nano*, 2013, **7**, 2106–2113.
54 Z. Wang, D. O. Carlsson, P. Tammela, K. Hua, P. Zhang, L. Nyholm and M. Strømme, *ACS Nano*, 2015, **9**, 7563–7571.
55 M. M. Hamedi, A. Hajian, A. B. Fall, K. Hkansson, M. Salajkova, F. Lundell, L. Wgberg and L. A. Berglund, *ACS Nano*, 2014, **8**, 2467–2476.
56 M. Hsieh, C. Kim, M. Nogi and K. Suganuma, *Nanoscale*, 2013, **5**, 9289–9295.